Journal of Luminescence 202 (2018) 450–460

Contents lists available at ScienceDirect

Journal of Luminescence

journal homepage: www.elsevier.com/locate/jlumin

A detailed aging analysis of MPO_4:X (M = Y^{3+}, La^{3+}, Lu^{3+}; X = Bi^{3+}, Pr^{3+}, Gd^{3+}) due to the Xe excimer discharge

Mike Broxtermann[a,*], Lena Marie Funke[b], Jan-Niklas Keil[a], Hellmut Eckert[b,c], Michael Ryan Hansen[b], Andries Meijerink[e], Ting Yu[e], Norbert Braun[d], Thomas Jüstel[a,*]

[a] Department of Chemical Engineering, Münster University of Applied Sciences, Stegerwaldstraße 39, D-48565 Steinfurt, Germany
[b] WWU Münster, Institut für Physikalische Chemie, Corrensstraße 30, D-48149 Münster, Germany
[c] Universidade de Sao Paulo, Instituto de Física de Sao Carlos, Sao Carlos, Sao Paulo 05508-020, Brazil
[d] GVB Solutions in Glass, Nordstern Park 2, D-52134 Herzogenrath, Germany
[e] Debye Institute for Nanomaterials Science, Universiteit Utrecht, Princetonplein 1, 3584 CC Utrecht, The Netherlands

ARTICLE INFO

Keywords:
Ns^2 luminescence
Phosphorus
UV phosphors
Lamp aging
Xe excimer discharge
VUV spectroscopy
Temperature and time dependent spectroscopy
Decay constants
Solid state NMR
EPR Spectroscopy

ABSTRACT

Phosphate hosts doped with luminescent ions are widely applied for efficient spectral conversion in light emitting devices. However, in Xe discharge lamps a rapid degradation of light output is observed indicating a decrease in the efficiency of conversion of the VUV output of the Xe discharge. This work aims at providing a better understanding of the degradation mechanism. We summarize peculiar findings made within a survey of different inorganic UV emitting phosphors of the MPO_4:X (M = Y, La, Lu; X = Bi, Pr, Gd) type regarding their stability under operation in a dielectric barrier Xe excimer discharge lamp. Test lamps containing these phosphors as a particle layer coating onto the inner wall of the lamp vessel suffer from a rapid degradation which was monitored by the loss of UV radiation output during lamp operation. The thus aged materials were recovered and further analysed by optical spectroscopy. It turned out that the aged materials do not only exhibit a new broad absorption in the UV/visible range, which explains the rapid decline of radiation output during lamp operation, but also that all aged materials show photoluminescence in the red upon exposure to UV radiation. It is argued that this luminescence originates from phosphorus in the oxidation state +III (configuration: [Ne]3 s^2) which is present as a point defect. These defects are formed when the respective materials are aged in direct contact with the Xe excimer discharge within the lamp discharge vessel. This detailed study of phosphor aging by means of VUV luminescence spectroscopy as well as temperature and time dependent luminescence spectroscopy and solid state EPR spectroscopy points to the existence of phosphorus +III ([Ne]3 s^2) which shows characteristic ns^2 luminescence which has not been reported before.

1. Introduction

For over 70 years ortho-phosphates and halophosphates have been widely applied as hosts for luminescent materials due to their high chemical stability and ease of synthesis [1,2]. In the 1940s halophosphates doped with Sb^{3+} and Mn^{2+} became the most widely used phosphor in fluorescent tubes. After the proposal of using a trichromatic phosphor blend to achieve colour 80 fluorescent lamps by Koedam and Opstelten, Verstegen et al. introduced another halophosphate as a blue emitting phosphor ($Sr_5(PO_4)_3Cl:Eu^{2+}$) for these trichromatic fluorescent lamps [3,4]. For applications as a green emitter for the trichromatic phosphor blend $LaPO_4$:Ce,Tb was developed somewhat later [5]. Owing to the higher stability of the rare earth activated phosphors as well as their higher efficacy the old halophosphate fluorescent lamps were replaced by trichromatic fluorescent lamps in the late 20th century [6]. The main problem of phosphate phosphors in fluorescent lamps is their pronounced Hg consumption compared to aluminate type phosphors or Y_2O_3:Eu. This observation was also made for the UV emitting phosphors YPO_4:Ce and $LaPO_4$:Ce, which causes the rather short operational lifetime of UV lamps used for tanning purposes [7,8].

The ortho-phosphates $LuPO_4$ and YPO_4 doped by the RE elements Ce^{3+}, Pr^{3+}, or Nd^{3+} are also promising scintillator materials [9] due to their radiation hardness, short decay time, and rather high photon yield [10]. Recently, these materials were also proposed for the use as radiation converters for fluorescent Xe excimer discharge lamps [11,12]. Dielectric barrier Xe excimer discharges are applied in plasma displays and for VUV lamps where 172 nm radiation is converted to UV-C

* Corresponding authors.
E-mail addresses: mike.b@fh-muenster.de (M. Broxtermann), tj@fh-muenster.de (T. Jüstel).

https://doi.org/10.1016/j.jlumin.2018.05.056
Received 3 April 2018; Received in revised form 22 May 2018; Accepted 23 May 2018
Available online 26 May 2018
0022-2313/

radiation which can be exploited for surface, air, and water purification [13].

Doped ortho-phosphates $LnPO_4$:M (Ln = Y, Gd, Lu; M = Bi, Ce, Pr, Nd) are effective UV radiation sources, whose emission spectrum is solely dependent on the applied phosphor or phosphor blend. Pr^{3+}, Nd^{3+}, or Bi^{3+} doping produces emission in the range 190–280 nm, while Ce^{3+} or Gd^{3+} doping result in UV-B or UV-A emitting materials, e.g. YPO_4:Ce (345 nm), YPO_4:Gd (312 nm) or $LaPO_4$:Ce (312 nm). Very efficient UV-C emitters are YPO_4:Nd (193 nm), YPO_4:Pr (235 nm), YPO_4:Bi (241 nm), $LaPO_4$:Pr (225 nm), and $LuPO_4$:Pr (235 nm). However, it must be kept in mind that also many other inorganic hosts doped by Pr^{3+} show efficient UV-C or UV-B emission, such as the Whitlockite $Ca_9Lu(PO_4)_7$:Pr [14] or garnet type ortho-silicates $Ca_3Sc_2Si_3O_{12}$:Pr [15].

The high quantum yield, good overlap with the germicidal action curve, and low thermal quenching effects of YPO_4:Bi and YPO_4:Pr make these materials suitable for applications as UV-C emitters in Xe excimer discharge lamps for disinfection [16]. Unfortunately, both materials show tremendous degradation during the course of lamp operation, so that their commercial use is not in immediate reach [17]. A well-established way to improve the phosphor stability in discharge lamps or emissive displays are particle coatings. It was already proven that a γ-Al_2O_3 coating onto YPO_4:Bi particles will improve the stability in Xe discharge lamps, by forming a very homogeneous nanoscale layer on the grains [17]. However, the stability improvement was not sufficient to make these lamps competitive with respect to the lifetime of 253.7 nm emitting low-pressure Hg discharge lamps. At present, the details of the degradation mechanism of ortho-phosphates in Xe excimer discharge lamps and the corresponding roles of the activator and the host are not known.

It is the aim of this work to provide insight in the degradation mechanism of rare earth or Bi^{3+} activated ortho-phosphate type phosphors in Xe excimer discharge lamps. To this end, a series of Xe excimer lamps with different phosphor coatings were made and operated for several hundred hours. Physical and chemical properties of the as-made and degraded ortho-phosphate type phosphors were investigated and compared. The insights obtained form the basis of a strategy for future phosphor development and lamp design.

2. Experimental Section

2.1. Material Syntheses

2.1.1. Synthesis of μ-scale YPO_4, $LaPO_4$, and $LuPO_4$

All microscale powders were made by solid state synthesis starting from Ln_2O_3 (Ln = Y, La, Lu), $(NH_4)H_2PO_4$ and by using LiF as a flux. After thoroughly blending the materials in an acetone slurry, the powder blends were transferred into corundum crucibles and subsequently annealed at 1000 °C for 4 h in ambient atmosphere. The obtained sinter cakes were thoroughly ground, washed with demineralized water and then dried in a drying furnace at 80 °C at a pressure of 10^{-3} mbar for 8 h. Finally, the obtained white powders were sieved through a nylon sieve with a mesh width of 36 μm to remove remaining agglomerates. Table 1 lists the masses and molar amounts of the starting materials used.

2.1.2. Synthesis of μ-scale YPO_4:Bi^{3+} (0.5%) and YPO_4:Gd^{3+} (1%)

The educts Y_2O_3 (150.0 g, 0.665 mol) and Bi_2O_3 (1.555 g, 3.338 mmol) for the synthesis of YPO_4:Bi or Y_2O_3 (150.0 g, 0.665 mol) and Gd_2O_3 (2.420 g, 6.676 mmol) for the synthesis of YPO_4:Gd were suspended into demineralized water. Then concentrated H_3PO_4 (161.641 g, 1.402 mol) was added under intimate stirring within 24 h. The obtained slurry was dried in a rotary evaporator before 1 wt.-% of LiF was added as a flux and the blend was ground to homogeneity. The blend was placed into a corundum crucible and annealed at 1000 °C for 4 h at ambient atmosphere. The obtained sinter cake was ground and suspended into 1000 ml HNO_3 (65%) and 4000 ml demineralized water and stirred at 60 °C for 6 h. Afterwards, the powder was separated by filtration and washed with demineralized water until the wash water was neutral. Subsequently, the powder was dried in a drying furnace at 80 °C at a pressure of 10^{-3} mbar for 8 h. Finally, the powder was milled to obtain an appropriate particle size ($d_{50} \approx 5 - 6$ μm). To this end, the powder was filled into a 2000 ml PE bottle, 203 g 1-Propanol as well as 2330 g YTZ balls were added and the obtained slurry was rolled for 6 h hours on a roller bench. After the milling process the obtained fine white powder was annealed at 800 °C for 2 h in a corundum crucible to heal (surface) defects due to the milling process. Finally, the obtained white powders were sieved through a nylon sieve with a mesh width of 36 μm to remove remaining agglomerates.

2.1.3. Synthesis of μ-scale YPO_4:Pr^{3+} (1%)

The educts Y_2O_3 (150.0 g, 0.665 mol) and Pr_6O_{11} (1.021 g, 2.225 mmol) were suspended into demineralized water. Then concentrated H_3PO_4 (161.641 g, 1.402 mol) was added under intimate stirring within 24 h. The obtained slurry was dried in a rotary evaporator before LiF was added and the blend was subsequently ground to homogeneity. The blend was placed into a corundum crucible and annealed at 1000 °C for 4 h in a CO atmosphere to ensure a complete reduction of present Pr^{4+} to Pr^{3+}. The obtained sinter cake was ground and suspended into 1000 ml HNO_3 (65%) and 4000 ml demineralized water and stirred at 60 °C for 6 h. Afterwards, the powder was separated by filtration and washed with demineralized water until the effluent water was neutral. Subsequently, the powder was dried in a drying furnace at 80 °C at a pressure of 10^{-3} mbar for 8 h. Finally, the powder was milled to obtain an appropriate particle size ($d_{50} \sim 5 - 6$ μm). To this end, the powder was filled into a 2000 ml PE bottle, 203 g 1-Propanol as well as 2330 g YTZ balls were added and the obtained slurry was rolled for 6 h hours on a roller bench. After the milling process the obtained fine white powder was annealed at 800 °C for 2 h in a corundum crucible to heal surface defects due to the milling process. Finally, the obtained white powders were sieved through a nylon sieve with a mesh width of 36 μm to remove remaining agglomerates.

2.2. Xe excimer lamp construction and aging

2.2.1. Phosphor paint preparation

The inner side of the quartz vessel of the Xe neat excimer discharge lamp bodies were coated by applying a phosphor paint which is based on a 1:1 mixture of butylacetate/ethylacetate as dispersing agent which is charged with 5 wt.-% cellulose nitrate as binder. The resulting slightly viscous homogeneous solution is then charged with 20 wt.-% of the respective phosphor powder and agitated by using a roller bench

Composition	Y_2O_3	Lu_2O_3	La_2O_3	$(NH_4)H_2PO_4$
YPO_4 (25 g, 136.0 mmol)	15.36 g (68.0 mmol)	–	–	15.64 g (136.0 mmol)
$LuPO_4$ (25 g, 92.6 mmol)	–	18.42 g (46.3 mmol)	–	10.65 g (92.6 mmol)
$LaPO_4$ (25 g, 111.6 mmol)	–	–	18.18 g (55.8 mmol)	12.84 g (111.6 mmol)

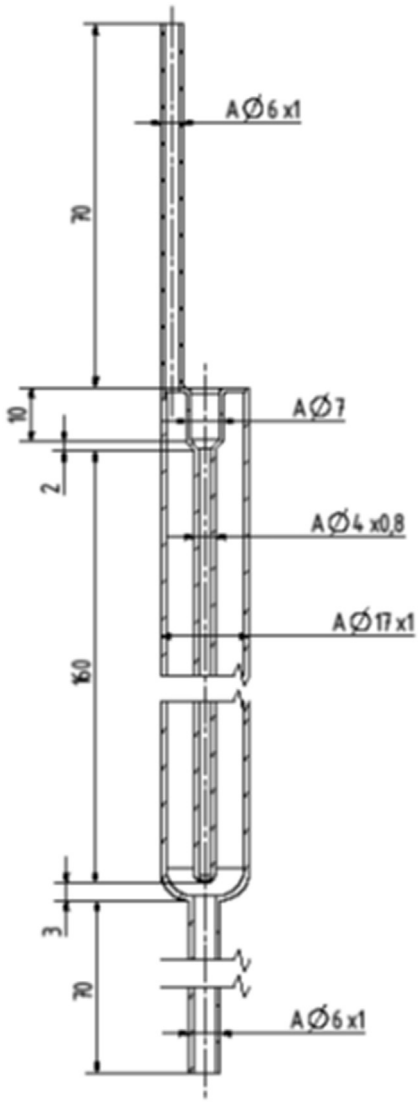

Fig. 1. Technical scheme of a Xe excimer discharge lamp.

until a homogeneous suspension is achieved. The resulting suspension is then sieved through a 36 μm sieve. The filtrated suspension is then stored under continuous agitation on a roller bench to prevent precipitation or aggregation.

Fig. 1 presents a technical drawing of the lamp quartz body (synthetic quartz, Heraeus) including 6 mm diameter and 70 mm length quartz tubes fused to the top and bottom part, which are used to aid in the coating and the later gas filling steps. The discharge vessel itself exhibits an outer diameter of 17 mm and a wall thickness of 1 mm at an overall length of 175 mm. The inner quartz tube is 4 mm wide, exhibiting a wall thickness of 0.8 mm.

Each lamp body was weighed before any coating is applied. The respective phosphor paint, prepared as described above, was sucked into the vertically aligned lamp through the 6 mm wide tube fused to the lamp bottom applying a small vacuum until the whole body is filled. Vacuum was then released and the paint is allowed to flow out again. A gentle flow of preheated air was then applied to dry the paint that is adhering to the discharge vessel walls. This procedure was repeated once, following horizontal 180° rotation of the lamp body before the whole body was weighed out again in order to determine the average coating weight. Any organic components remaining from the paint are removed via heating the coated body to 500 − 600 °C for 1 h.

After a lamp body was successfully coated with a respective phosphor material, the bottom 6 mm diameter tube was flame-sealed. The coated lamp body was then heated to 500 − 600 °C for 0.5 h at ambient pressure once again before it was connected to the gas filling apparatus via the remaining 6 mm diameter quartz tube at the top part. Prior to the filling with 200 − 500 mbar of Xe gas (Westfalengas 99.99%), the lamp body experienced a final preheating step at 500 − 600 °C upon applying a vacuum of 10^{-3} mbar for 1 h. Subsequently, the as-filled lamp was provisionally ignited in order to monitor the gas filling for impurities (e.g. Oxygen) via observation of the apparent discharge colour before it is separated (by flame sealing) from the upper quartz tube connected to the filling apparatus. The inner tube of the as coated and gas filled lamp body was then filled with stainless steel powder as inner electrode, which was afterwards connected to a flexible electronically shielded cable. Eventually, stainless steel netting may be stripped over the discharge vessel, to act as an outer electrode. All the as prepared lamps were finally tested for appropriate ignition behaviour.

2.3. Lamp lifetime experiments and driving scheme

Phosphor-coated lamps to be tested with respect to their maintenance in operation and their long term stability were fitted into a mounting centred within a closed 50 mm diameter PMMA vessel, which was constantly purged by flowing water. The cooling water was continuously circulated and amounts to 8 l of supply water exhibiting an electrical conductivity, which was typically higher than 100 μS/cm and was tested for its conductivity and UV transmission prior and repeatedly during the lifetime experiments. For a usual lifetime experiment, such Xe excimer lamps were continuously operated for 500 h at least.

UV radiation output was recorded with an Avantes spectrometer (AVASPEC-ULS2048, detection range 200 − 1000 nm) using a 25 μm slit, grating 300 lines/mm, and 300 nm blaze, to which a 200 μm quartz fibre (solarisation resistant, NA 0.22) was connected for radiation guiding. In order to specify the measurement position, the quartz fibre comprised an adapter to affix the fibre to the lamp surface at a defined position attached onto lamp surface.

UV outputs were measured repeatedly after certain lamp operation periods, over the total operation period of 500–700 h. The spectra were recorded between 200 and 900 nm and then subsequently normalized to the integrated Xe lines between 820 and 830 nm. Since the ratio of the Xe line emission in the NIR to the VUV emission of the Xe excimers remains constant during lamp operation, the ratio of the integrated phosphor spectrum in the UV range to the integrated Xe line spectrum in the NIR yields corrected integral emission intensities. The change over time of this number yields the degradation curves.

Efficient lamp driving is achieved by using a high voltage narrow unipolar fly back pulse driver (3.8 kV, 90 kHz) [1]. The voltage and current profiles of the used power supply units are given within Fig. 2. With respect to the as displayed driving scheme, the Xe excimer discharge lamp is supplied with a power input of roughly 11 W resulting in a power consumption of about 0.73 W/cm lamp or discharge lengths, respectively.

2.4. Photoluminescence spectroscopy

PL emission as well as excitation spectra were recorded on an Edinburgh Instruments FSL 920 spectrometer equipped with a 450 W Xe arc lamp, mirror optics for powder samples and a cooled (−20 °C) single-photon counting photomultiplier from Hamamatsu (R2658P). For PL decay kinetics a μF 920 H Xe flash lamp (100 W) from Edinburgh Instruments was used as excitation source. Temperature dependent PL measurements in the range from 78 to 500 K were carried out applying an Oxford Instruments cryostat MicrostatN2. The cooling agent was liquid nitrogen. Accuracy of the temperature measurement was set to ± 3 K and the stabilization time to 30 s.

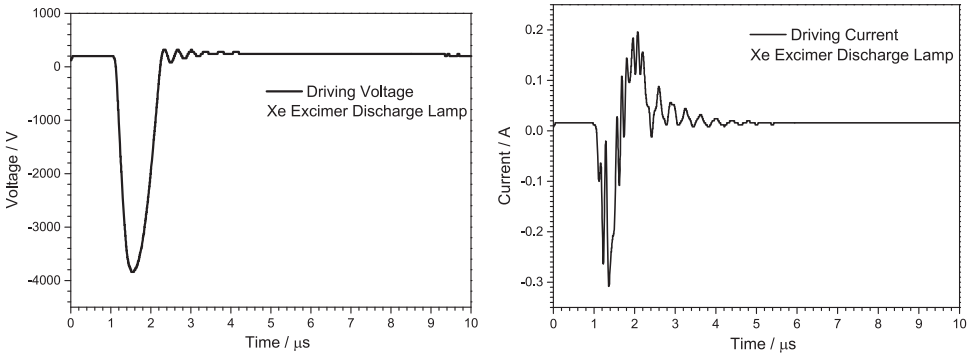

Fig. 2. Driving voltage and current as supplied by the used power supply units for Xe excimer discharge lamp operation in lifetime testing.

The correction file for the emission spectra was obtained from a tungsten incandescent lamp certified by the National Physical Laboratory, Teddington, UK. Diffuse reflection (DR) spectra were recorded on a spectrometer of the same model, equipped with a "spectralon" coated integration sphere. $BaSO_4$ (99.998%, Sigma-Aldrich) was used as a reflection standard. Analysis and handling of data was carried out with the F900 program issued by Edinburgh Instruments.

2.5. Reflection spectroscopy

Reflection spectroscopy was performed on an Edinburgh Instruments FL920 spectrofluorimeter equipped with a custom made Spectralon coated integrating sphere. Excitation was provided by a 450 W Xe arc lamp. The device is operated with two TMS300 (Czerny-Turner Optics) monochromators equipped with 1800 g/mm gratings each and a Peltier cooled (−20 °C) R928 single photon PMT (Hamamatsu). Optical grade $BaSO_4$ (99.998% Sigma-Aldrich) was used as a white standard and thus set to 100% reflectance.

2.6. VUV luminescence spectroscopy

The VUV spectrometer used consists of an Edinburgh Instruments FL920 spectrofluorimeter, which is equipped with a VUV excitation arrangement. This VUV excitation arm consists of a D_2 discharge lamp (DS-775), an Acton Research VM-504 VUV-monochromator as well as a mirror based focusing unit. The monochromator is equipped with manually controlled a micrometre-screw entrance and exit slit and of 1200 grooves per millimetre (g/mm) and a 2400 g/mm gratings. The VUV monochromator and the whole focusing unit are evacuated by a directly flanged turbo drag pump to realize a pressure of about 1.0×10^{-5} mbar. The D_2 lamp irradiates into the optical path of the evacuated monochromator through an MgF_2 window. The distance between the focusing unit, capped with another MgF_2 window and the sample which is placed in the unevacuated FL900 sample chamber, is constantly flooded with a dry stream of N_2 to ensure sufficient and stable VUV/UV exposure of the sample material. Sample emission is measured in a fixed 90° arrangement. The detection branch consists of a convex quartz collection lens, a Czerny-Turner Optics TMS300 monochromator equipped with a 1800 g/mm grating and a photomultiplier tube (PMT, Hamamatsu R928) running in single photon counting mode which is constantly kept at − 20 °C by Peltier cooling. All measurements were conducted on thoroughly powdered samples, which were placed in circular sample holders crafted from spectralon. A correction file for the emission spectra was obtained from a D_2 (UV range) and tungsten incandescent lamp (near UV—near IR-range) certified by NPL National Physical Laboratory, Teddington, UK.

Emission spectra were recorded upon 160 nm excitation by using the 1200 g/mm grating excitation, the 1800 g/mm emission grating, excitation slit widths corresponding to 2 nm and emission slit widths corresponding to 1 nm spectral resolution. The measurements of excitation spectra were conducted using the 2400 g/mm excitation and 1800 g/mm emission grating, excitation slit widths of 1 nm and emission slit widths of 2 nm. The measured uncorrected excitation raw spectra were divided by the spectrum of an excitation standard sample of Sodium salicylate (NaSal) (99.5%, Merck Millipore).

2.7. Solid state EPR measurements

Continuous-wave (CW) solid state EPR spectra were measured on a Bruker EMXnano X-band EPR spectrometer operating at a microwave frequency around 9.6 GHz. CW spectra were recorded as a function of the magnetic field strength in the range from 0.5 to 4.5 kG. The samples were filled inside 4 mm inner diameter quartz tubes. The samples were measured at ambient temperature and at 90 K using the variable temperature unit (ER 4141VT). For the acquisition of all the CW EPR spectra of YPO_4, YPO_4:Bi, and YPO_4:Pr a sweep rate of 96 mG/s and a time constant of 1.28 ms were used. The YPO_4:Gd spectra were measured with a sweep rate of 20 G/s. Depending on the sweep width 1200 − 14,000 points were recorded. The modulation frequency was set to 100 kHz and modulation amplitudes of 1–5 G were used. A discrimination of EPR signals based on their saturation behaviour was performed by altering the microwave power between 0.08 and 1.26 mW. Spectral simulations for $LaPO_4$ were performed using the Aniso-SpinFit program within the Bruker Xenon software package.

3. Results and discussion

As-made non doped $LnPO_4$ (Ln = Y, La, Lu) as well as YPO_4 samples doped by Pr^{3+}, Gd^{3+}, or Bi^{3+} are brilliant white powders due to the wide band gap of the host material, which are reported to be 9.2 eV (YPO_4), 8.64 eV ($LaPO_4$), and 9.3 eV ($LuPO_4$), and the intra band gap location of the respective energy levels of the dopants, which have excited states that are typically in the UV range [18–21]. Consequently, the quality of all $LnPO_4$ samples discussed in this work was determined by reflection spectroscopy vs. $BaSO_4$ (supplementary information S 1–S 6). In addition, all phosphor samples used were investigated with respect to phase purity, which was revealed by powder x-ray diffraction before the lamps were mounted. It turned out that applied materials for lamp making were single phase and those materials recovered from aged lamps show neither a change of the powder x-ray diffraction patterns (see supplementary material S 7–S 12) nor of the X-ray photoelectron spectra (see supplementary material S 17 for $LuPO_4$).

Optical spectroscopy of all materials proves the presence of efficient photoluminescence upon 160 nm excitation. Fig. 3 compares the 160 nm excited PL spectra with the PL spectrum of the blue emitting plasma display panel (PDP) phosphor $BaMgAl_{10}O_{17}$:Eu (quantum yield of about 96% if one assumes that the absorption strengths upon 160 nm excitation are of similar magnitude for both materials [22].)

The PL excitation spectra of all discussed YPO_4 phosphors feature a relatively narrow excitation band at 152 ± 2 nm (8.2 eV) which we, in

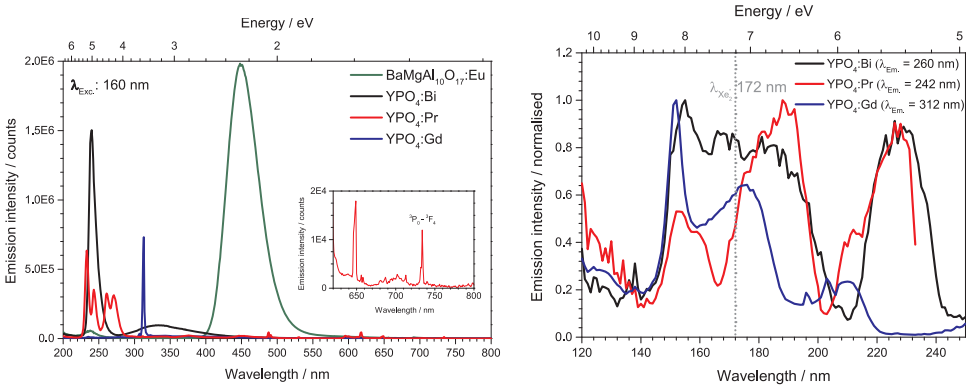

Fig. 3. Emission spectra upon 160 nm excitation of the investigated UV phosphors compared to the blue emitting plasma display panel phosphor $BaMgAl_{10}O_{17}$:Eu (left image) and respective excitation spectra (right image). The doted grey line in the excitation spectra plot marks the excitation peak wavelength, which is given in Xe excimer related applications due to Xe excimer emission.

Table 1
Stokes Shift and the location of the excitation and emission bands of the YPO_4:M (M = Pr, Gd, Bi) phosphors and of the VUV reference material BAM:Eu [28].

As-made phosphors	Excitation bands [nm]	Emission bands [nm]	Stokes Shift [eV]
$BaMgAl_{10}O_{17}:Eu^{2+}$ (reference)	170, 200, 250, 300, 340, 390	453	0.44
YPO_4:Pr	152, 155, 190, 225	235, 243, 260, 270	0.23
YPO_4:Gd	152, 175, 202, 272, 308	312	0.05
YPO_4:Bi	154, 170, 185, 225	241, (335)	0.37

accordance with recent literature, assign as a conduction band charge transfer (CB-CT) between the involved activator ground state and the host material conduction band. YPO_4:Bi exhibits two additional excitation bands due to electronic interconfigurational $[Xe]5d^{1\circ}4f^{14}6s^2$ – $[Xe]\ 5d^{10}4f^{14}6s^16p^1$ transitions by Bi^{3+}. We observe one poorly resolved excitation band around 180 nm (6.9 eV) corresponding to the $^1S_0 \rightarrow {}^1P_1$ transition (C band) extende by Bi^{3+} - YPO_4 CB-CT, and another lower energetic excitation band at 225 nm (5.5 eV) corresponding to the $^1S_0 \rightarrow {}^3P_1$ transition (A band) [21,23]. The PL emission spectrum of YPO_4:Bi is governed by a relatively narrow emission band ranging from approximately 225 to 275 nm and peaking at around 241 nm (5.2 eV) which originates from the interconfigurational transition $[Xe]\ 5d^{10}4f^{14}6s^16p^1$ – $[Xe]\ 5d^{10}4f^{14}6s^2$. It is more precisely assigned to the electronic transition $^3P_1 \rightarrow {}^1S_0$, typical for Bi^{3+} as an activator cation (at room temperature, at low temperatures $^3P_0 \rightarrow {}^1S_0$ emission is observed at the same wavelength) [24]. Additionally, YPO_4:Bi exhibits a second, lower energetic broader emission band, with an onset at 275 nm (4.5 eV), a peak at 335 nm (3.7 eV) and gradually diminishing in intensity towards 500 nm. This band was originally assigned by Blasse as the main band in 1968 [24]. The origin of that low energy emission band, however, remains an issue of discussion in the recent literature and was on the one hand attributed to a Y^{3+}-Bi^{3+} CT by Boutineaud et al. whereas Srivastava et al. explained the emission band to origin from Bi-pair or clusters [25,26]. The PL excitation spectrum of YPO_4:Gd reveals excitation bands peaking at 175 (7.1 eV), 210 nm (5.9 eV) and some sharp lines around 200 nm (6.1 eV), 272 nm (4.6 eV) and 308 nm (4.0 eV). The origin of the broad bands is not clear as Gd^{3+} has no allowed f-d or charge transfer transitions between 150 and 250 nm. The sharp lines are assigned to $^8S_{7/2} \rightarrow {}^6G_J$ (200 nm), $^8S_{7/2} \rightarrow {}^6I_J$ (275 nm), and $^8S_{7/2} \rightarrow {}^6P_J$ (308 nm). The emission spectrum measured on YPO_4:Gd shows typical sharp 4–4f emission lines originating from the $^6P_{7/2} \rightarrow {}^8S_{7/2}$ electronic transition typical for Gd^{3+}. The respective narrow emission line shows a maximum at 312 nm (3.97 eV). YPO_4:Pr exhibits a PL excitation spectrum which reveals excitation bands corresponding to $[Xe]4f^2$-$[Xe]4f^15d^1$ electronic transition of the trivalent Pr^{3+} peaking at 155 nm (8.0 eV), 190 nm (6.5 eV) and 225 nm (5.5 eV). The PL emission spectrum is governed by a typically structured UV-C emission band originating from the $[Xe]4f^15d^1$-$[Xe]4f^2$ electronic transition, more precisely a transition of the $4f^15d^1$ excited state to the ^3H_J ground state manifold. The spectra are in good agreement with reports in the literature [27]. Additional emission lines peaking in the visible spectral range originate from Pr^{3+} centred $[Xe]\ 4f^2$-$[Xe]4f^2$ (f-f) electronic transitions $^3P_0 \rightarrow {}^3H_J$ and ^3F_J. With regard to the targeted application as VUV to UV-C converting phosphors, efficiently transforming the UV-C excimer discharge emission peaking around 172 nm (7.2 eV) into the UV-C or UV-B, all herein discussed phosphors exhibit nicely matching PL excitation as well as photoemission spectra. Table 1 summarizes the herein sicusses excitation- and emission band positions as well as the resulting Stokes Shifts.

Fig. 4 presents the emission spectra which were measured from YPO_4:Bi, YPO_4:Pr, and YPO_4:Gd containing Xe excimer discharge lamps for operation conditions as described earlier. In order to give a first rough impression about the lamp performance over operation time Fig. 4 also shows a comparison of the initial lamp output near the beginning and the end of the lifetime testing (typically around 700 h). In addition to the characteristic emission lines and bands originating from the incorporated phosphor species, all the lamp spectra show a NIR-line emission in the spectral range 800–1000 nm after aging. This line emission originates from the Xe plasma discharge and is caused by emission of atomic Xe^0 which is excited by collisions with electrons within the discharge filaments. The respective lines are marked with capital letters A to H in Fig. 4. In order to present an authentic lamp spectrum which meets the demands of completeness regarding the true spectral power distribution it would have been necessary to monitor for wavelengths shorter than 200 nm, as the discharge vessel, although internally coated with phosphor, may transmit a certain amount of VUV irradiation originating from the Xe excimer discharge. Within the present study this measurement was not possible owing to instrumental limitations.

Remarkably, all the measured lamps regardless of the applied phosphor (YPO_4:Bi, YPO_4:Pr, or YPO_4:Gd) exhibit a distinct reduction of their UV output after aging, as indicated by the spectral comparison of Fig. 4. For the YPO_4:Bi and YPO_4:Pr lamps, the integrated intensity over the UV range (200 – 380 nm) are reduced by 64% and 69%, respectively, after 768 h of operation. In the case of the YPO_4:Gd lamp an 88% reduction after 600 h of operation was observed. The decrease in UV output was monitored by recording the lamp emission spectra as a function of operation time. Since the intensity ratio of the Xe NIR line

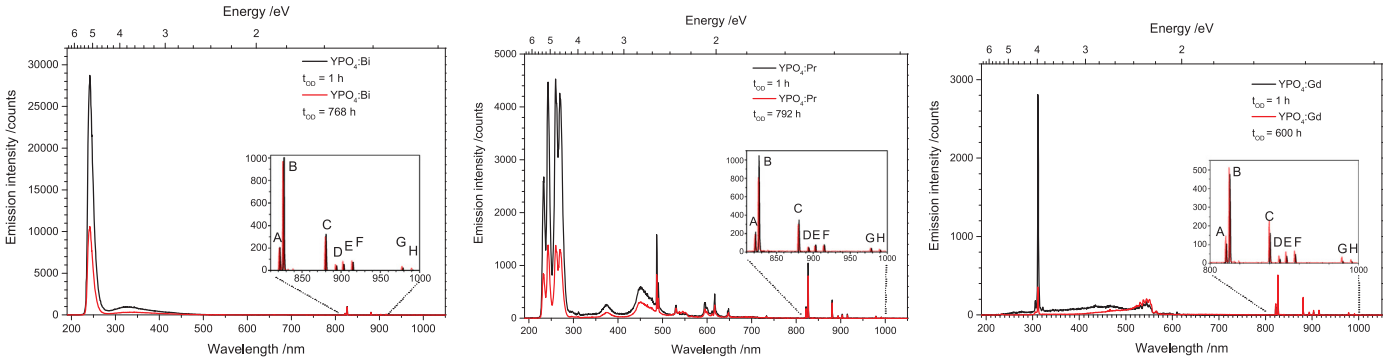

Fig. 4. Emission spectra as taken of an YPO_4:Bi (left), an YPO_4:Pr (middle), and an YPO_4:Gd comprising Xe excimer discharge lamp (right) after operation times of 1 and ≥ 600 h.

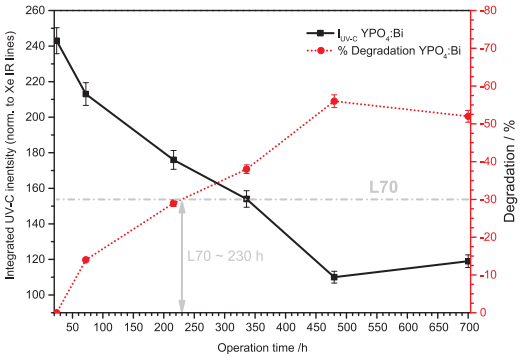

Fig. 5. Integrated and corrected (to IR line A and B line integral) UV-C output of a YPO_4:Bi comprising Xe excimer discharge lamp over operation time (black, solid) and the correlating degradation calculated from the respective UV-C integrals set into relation to the UV-C integral after 24 h of operation as 100% reference.

emission to the VUV emission of the Xe excimer discharge (172 nm) remains constant during lamp operation, we used the integral over line A and B (920 – 930 nm) in order to correct the integrated lamp UV emission to take a possible decline in initial plasma discharge intensity into account. To remove data distortions arising from any intensity changes originating from the excimer discharge upon the monitored data, we calculated the ratio of the integrated phosphor spectrum in the UV range or in a certain fraction of it to the integrated spectrum of the IR lines A and B. The resulting degradation curves for the YPO_4:Bi based Xe excimer discharge lamp are shown in Fig. 5. Additionally to the integrated and corrected integral over the UV-C range, Fig. 5 shows the corresponding degradation values calculated by relating the integrated and corrected UV-C intensities to the respective integrals for 24 h - operation (normalized to 100%). We defined an operation time of 24 h as the zero-degradation time standard t_0, as manufactured lamps typically feature a significant increase in their recorded radiation output within their first hours of operation, which tends to stabilize within a 24 h "burn-in period". The inserted grey line indicates the so-called L70 value, which is often used as a lifetime metric for many light sources, e.g. fluorescent lamps or LEDs. It is defined as the time by which a 30% decrease in output intensity has occurred with respect to its initial output intensity after t_0. For the YPO_4:Bi containing Xe excimer lamp, operated in H_2O (outer electron deficient lamp which is directly placed and operated in water, see lifetime experiment description in the experimental part), the L70 amounts to approximately 230 h of continuous operation. After 700 h of operation, the UV-C output decline has reached 52%. Comparable results (L70 = 230 − 250 h) were observed for YPO_4:Pr and YPO_4:Gd lamps. Considering that these results are already corrected for any output reduction caused by changes within the plasma discharge, this astonishing decline in UV-C output strictly points to a rapid and distinct degradation of the applied lamp discharge vessel and other involved essential components, such as the phosphor material.

This finding prompted us to carry out a detailed post aging analysis of the recovered phosphor powders. Thus, the aged lamps were opened, the phosphor material recovered by treatment with ethanol in an ultrasonic bath and subsequently dried at 80 °C at $1{\cdot}10^{-3}$ mbar for at least 6 h. These samples revealed a significantly reduced reflectance in the visible and in the UV range as depicted in Fig. 6. Also their emission intensities are significantly reduced, whereas peak positions and width remain unaltered. Based on the reduced reflectance over the respective wavelength domain (UV-C/B range), we attribute this reduction in UV yield to re-absorption processes. Furthermore, as documented in the supporting materials section, none of the recovered materials evidence any phase changes or formation of additional impurity phases. Interestingly, however, the aged YPO_4:Bi sample gives rise to a new absorption band at 480 nm (2.6 eV) not present in the initial material. Based on comparable observations made in Bi-doped silicate glasses, we tentatively attribute this new absorption to a reduction of Bi^{3+} to Bi^{2+} [29]. This conclusion is further supported by R. Awater et al., who report in the formation and luminescence of Bi^{2+} centres in YPO_4 upon electron trapping from the conduction band by Bi^{3+} centres [21].

For further insights into the degradation mechanism, we required an interpretation of additional strong absorption bands, which show up only after lamp operation. A strong indication that the host material rather than the activator ion is the main responsible factor for the degradation observed is given by the fact that the changes appear independent of the nature of the dopant ions. This conclusion is underlined by the fact that Gd^{3+} in particular is considered as a very redox stable activator ion and the spectra for Gd-doped YPO_4 show the same absorption bands in the UV.

These conclusions are further supported by the reflectance spectra of a non-doped YPO_4 sample before and after lamp operation (see Fig. 7). In this case, one observes a strong reduction of the reflectance below 600 nm which culminates in the UV-C range at about 250 nm. Based on these findings we conclude that the degradation process of YPO_4-based materials is predominantly governed by the modification of the host material rather than by the presence or change of the redox state of the activator ions. Only for YPO_4:Bi^{3+} a dopant-related absorption band is observed around 480 nm and assigned to Bi^{2+}.

To investigate if the VUV induced absorptions are related to structural transformations, PXRD and XPS measurements were done. As no phase transitions or impurity phases could be observed within the detection limits of our PXRD and XPS experiments (see supplementary information, S16, S17), we conclude that the changes in the reflection spectra must be due to specific defect species with rather large absorption cross sections.

As the discharge is in intimate contact with the phosphor layer, we hypothesize that the processes contributing to the phosphor

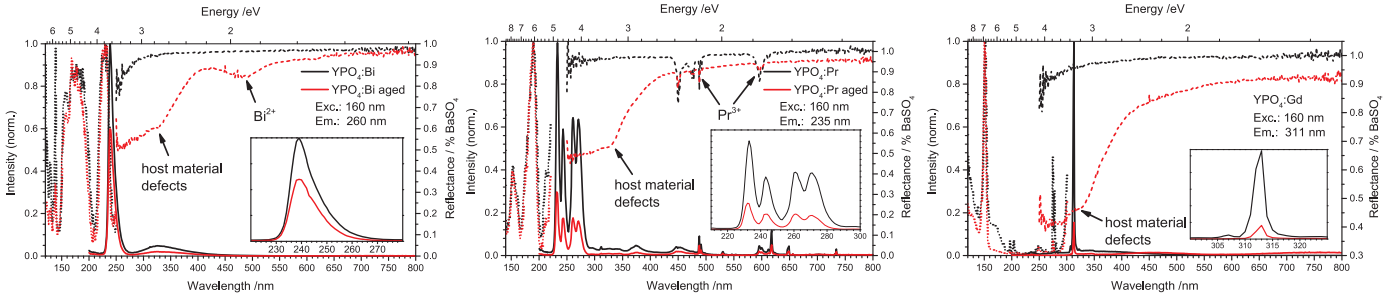

Fig. 6. Degradation behaviour of YPO_4:Bi, YPO_4:Pr, and YPO_4:Gd in an Xe excimer discharge lamp within 700 h lamp operation. VUV PL excitation and emission spectra as well as diffuse reflectance spectra measured from as synthesized phosphor powders as well as phosphor samples recovered after application within a Xe excimer discharge lamp.

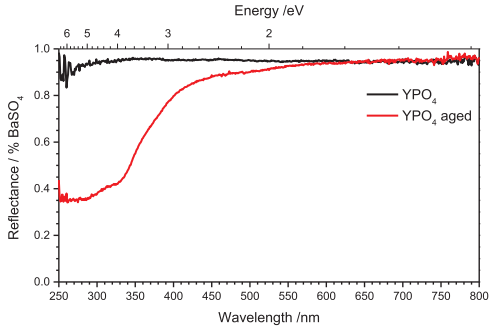

Fig. 7. Reflectance spectra of an as-made YPO_4 sample (black line) and an YPO_4 sample recovered after 567 h operation from a Xe excimer discharge lamp (red line).

degradation include (1) the up-take of hot electrons and (2) the sputtering of the phosphor surface by Xe cations resulting in a loss of oxygen. The latter process takes place if the phosphor surface is in the cathode mode in such AC driven lamps, which means that Xe cations are attracted by the surface giving rise to the so-called cathode fall which involves accelerated Xe^+ cations with kinetic energies within the range of some keV. The resulting formation of oxygen vacancies is supported by the observation of the gas discharge volume, which develops a green emission during lamp operation (see supporting information S13–S15). This green emission is attributed to "XeO* " species in accordance to literature [30,31]. The loss of oxygen from the phosphor layer points to the formation of Oxygen vacancies, which can be interpreted by the formation of PO_3^{3-}, featuring trivalent phosphorus (electron configuration [Ne]3 s^2).

This assumption is in line with the PL spectra of degraded phosphor powders as recovered from the respective lamps. Fig. 8 presents a temperature dependent series of PL emission and corresponding PL excitation spectra, as recorded for YPO_4:Bi, YPO_4:Pr, and YPO_4:Gd as well as for non-doped YPO_4. It turned out that excitation into the novel UV absorption bands of degraded doped YPO_4 (either Bi^{3+}, Pr^{3+}, or Gd^{3+}) and as well non-doped YPO_4 yields a very broad deep red/NIR emission band peaking between 650 and 800 nm, with an additional shoulder at 550 – 600 nm observed only at measurement temperatures below 175 K. In addition to the broad banded emission, the emission spectrum of YPO_4:Pr shows typical 4–4f emission lines originating from transitions from the ^3P_J manifold to the ^3H_J and ^3F_J states of Pr^{3+} upon 348 nm excitation (Table 2). The deep red emission band shows an excitation spectrum with two to three narrow bands with maxima located in the UV range. The positions of the excitation bands appear to be nearly independent on temperature although the structure visible at low temperature blurs with increasing temperature. A close look at the excitation and emission spectra of aged YPO_4:Bi (Fig. 8, left) reveals that the Bi dopant must be responsible for the excitation band located at 480 nm (2.6 eV). This is either caused by the PL of Bi^{2+} which contributes to the monitored broadbanded deep-red/NIR emission or by an energy transfer process between Bi^{2+} and the respective luminescent centre, which we propose to be a trivalent phosphorus species.

Another peculiar detail which is revealed by the excitation spectrum of YPO_4:Pr is the presence of Pr^{3+} related 4–4 f excitation lines at 449 (2.8 eV), 452 nm (2.7, $^3H_4 \rightarrow {}^3P_2$), 472 nm (2.6 eV), 474 nm (2.6 eV), 477 nm (2.6 eV), 488 nm (2.5 eV), and 491 nm (2.5 eV, $^3H_4 \rightarrow {}^3P_{0,1}$) upon monitoring the PL at 735 nm. We explain these excitation lines to origin from the observation of Pr^{3+} f-f luminescence, respective emission originating from the $^3P_0$ – $^3F_4$ transition of Pr^{3+} is observed at around 735 nm (see inset of Fig. 3, left). The recorded and herein presented PL excitation spectrum thus displays PL excitation bands of the new host related impurity centre as well as additional lines due to common Pr^{3+} luminescence.

Overall, the spectroscopic findings on the aged YPO_4 phosphors doped with Pr, Gd, or Bi and the comparison with aged non-doped YPO_4 strongly point to a degradation process of the host being in contact with the Xe excimer discharge. In order to further examine such hypothesis, we extended the research to other non-doped ortho-phosphates, viz. $LuPO_4$ and $LaPO_4$. $LuPO_4$ is isostructural to YPO_4 (Xenotime, tetragonal, space group $I4_1/amd$ (#141)) whereas $LaPO_4$ crystallizes in the monoclinic monazite type structure ($P2_1/n$ (#14)). Corresponding Xe excimer lamps were constructed, aged under analogous conditions after which the phosphor materials were recovered, and finally spectroscopically examined. Fig. 9 presents temperature dependent PL excitation and emission spectra for comparison with the results obtained on aged YPO_4 discussed above.

From Fig. 9 it is evident that the aged non-doped compounds YPO_4, $LuPO_4$, and $LaPO_4$ share crucial spectroscopic features, namely a set of distinct UV excitation bands which give rise to a very broad band photoluminescence, also peaking in the deep red spectral region. Table 3 summarizes the excitation and emission maxima.

Sputtering by $Xe^{+\cdot}$ as well as the impingement of electrons can cause the formation of colour centres. Again, we propose that this mechanism finally leads to the formation of P^{3+} centres, which is in line with a reduction of P^{5+} as the central ion of the PO_4^{3-} tetrahedra, which is the anionic building unit in YPO_4, $LuPO_4$ and $LaPO_4$. In Fig. 10 the energy level scheme of P^{3+} (an s^2 species) is shown on the left and excitation and emission spectra of an excimer aged sample of $LuPO_4$ are shown on the right. The excitation and emission bands are assigned based on this energy level scheme. The strong absorption is due to the spin-allowed and parity-allowed $^1S_0$–$^1P_1$ transition (C-Band). The splitting in the band can be due to crystal field splitting (the symmetry is lower than octahedral) and possibly a Jahn-Teller effect as is observed in the more familiar s^2 ions Pb^{2+} and Bi^{3+}. Following absorption in the $^1P_1$ level fast relaxation to the $^3P_{0,1}$ lowest excited state is followed by slow (spin-forbidden) emission to the $^1S_0$ ground state. The $^3P_0$–$^3P_1$ energy speration will be extremely small as spin-orbit coupling is weak for light elements as P. As a result, even at the lowest temperatures the $^3P_1$ state will be (partially) populated and emission from this level will dominate as the $^3P_0$–$^1S_0$ transition is more strongly

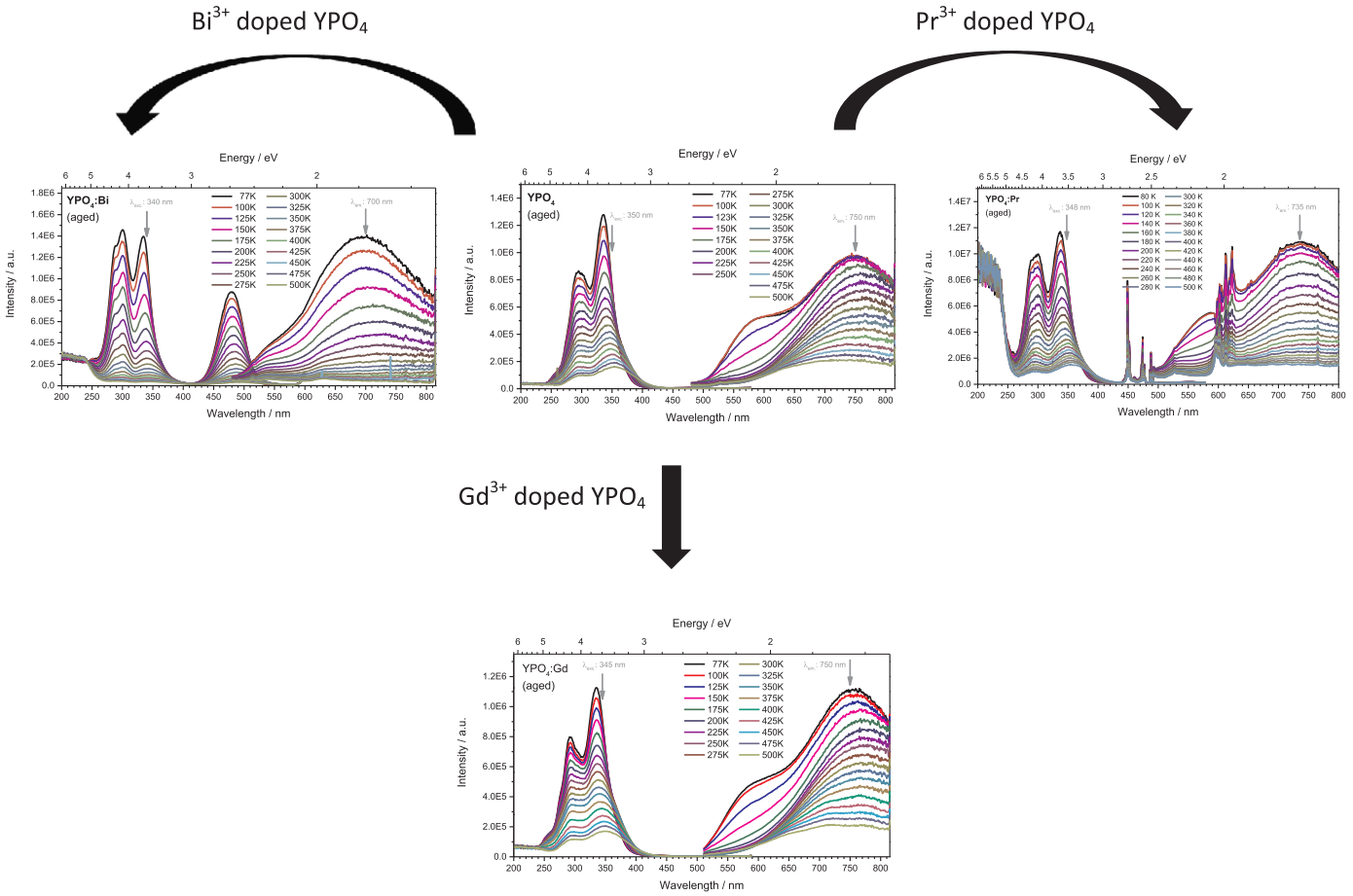

Fig. 8. Temperature dependent PL emission and excitation spectra of YPO_4:Bi, YPO_4, YPO_4:Pr, and YPO_4:Gd samples after aging within an Xe excimer discharge lamp and subsequent recovery measured between 80 and 500 K.

Table 2
PL excitation and emission maxima shown by YPO_4, YPO_4:Bi, YPO_4:Pr, and YPO_4:Gd samples aged in an excimer discharge lamp (measured at 77 K).

Aged phosphor	Excitation maxima at 77 K [nm]	Emission maxima at 77 K [nm]
YPO_4	297 / 395	~590 / 750
YPO_4:Bi	288 / 300 / 335 / 480	696
YPO_4:Pr	300 / 337/ 449*/ 452*/ 472*/ 474*/ 477*/ 488*/ 491*	598*/ 602*/ 605*/ 612*/ 617*/ 623*/ 735
YPO_4:Gd	291 / 335	~590 / 755

* indicates maxima originating from typical activator photoluminescence

Table 3
PL excitation end emission maxima exhibited by excimer lamp aged YPO_4, $LuPO_4$ and $LaPO_4$ at 70 K.

Aged compound	Excitation maxima at 77 K [nm]	Emission maxima at 77 K [nm]
YPO_4	297 / 395	~ 590 / 750
$LuPO_4$	268 / 291 / 325	720
$LaPO_4$	271 / 300 / 333	705

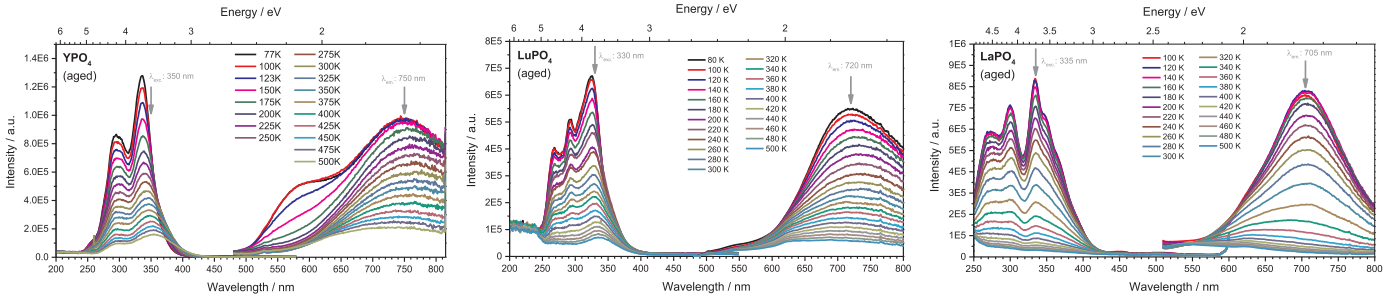

Fig. 9. Temperature dependent emission spectra of undoped YPO_4, $LuPO_4$, and $LaPO_4$ samples after aging in a Xe excimer discharge lamp and subsequent recovery (all spectra recorded between 77 and 500 K).

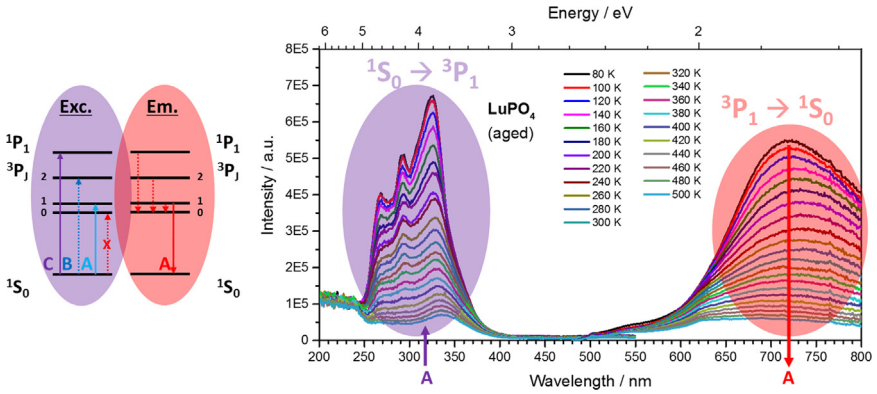

Fig. 10. Assignment of the observed spectral features in aged $LuPO_4$ to the expected transitions of a typical ns^2 ion (n = 3).

forbidden. Beyond that PL emission spectra taken from un-doped YPO_4 (Fig. 8, Fig. 9), was well as the doped materials YPO_4:X (X = Bi^{3+}, Pr^{3+}, Gd^{3+}, Fig. 8) reveal a shoulder peaking between 550 and 600 nm on the high energetic side of the deep-red $^3P_1$-$^1S_0$ emission band, which we assign to $^3P_2$-$^1S_0$ emission. This shoulder was shown to be visivle solely at measurement temperatures below 175 K as with increasing temperature a the non-radiative decay to emissive the $^3P_1$ state by phonon assisted relaxation is progressively promoted.

To further test our hypothesis that the deep red emission is related to P^{3+}, luminescence decay curves were recorded. In Fig. 11 the photoluminescence decay curves are shown for the 750 nm emission in aged YPO_4 for a temperature range between 100 and 500 K. At 100 K the emission life time is long, several ms. This is consistent with a spin-forbidden $^3P_1$-$^1S_0$ transition. Note that in the heavier s^2 ions (Sb^{3+}, Pb^{2+}, Bi^{3+}) emission lifetimes are typically on the order of µs. The stricter spin selection rule for the light P^{3+} s^2 ion because of weaker spin-orbit coupling can explain the long life times observed here. Upon raising the temperature, the decay becomes faster in the temperature regime where thermal quenching of the emission is observed. This is due to the increased non-radiative decay which accelerates the decay and reduces the light output. A detailed table listing the decay parameter obtained from performing double exponential fitting is to be found within the supporting information (S 18).

To examine the involvement of paramagnetic centres in the aging mechanism of the UV-emitting phosphors, continuous-wave (CW) X-band EPR spectra were measured on six different MPO_4 samples. Fig. 12 summarizes the CW X-band EPR spectra of YPO_4:Bi aged for 768 h, YPO_4:Pr aged for 888 h, of undoped YPO_4 aged for 432 h and of of undoped $LaPO_4$ aged for 456 h. The X-band EPR spectrum of aged $LaPO_4$ shows a lineshape typical of an anisotropic g-tensor. Similar lineshapes have been previously reported for radiation-induced defect centres in borophosphates [32], fluoride-phosphate glasses [33], and silicates [34,35]. The local magnetic field originates from a non-cubic environment that surrounds the paramagnetic centre, leading to a g-anisotropy when an external field is applied. Fig. 12 includes a simulation with g_x = 2.0057 (0.003), g_y = 2.0160 (0.012) and g_z = 2.0384 (0.034), subject to Gaussian distributions that account for small variations in the local interaction parameters.

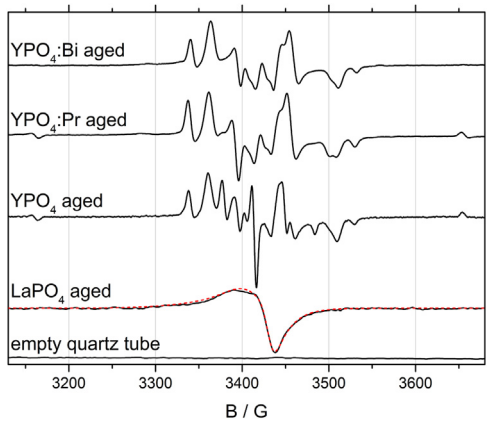

Fig. 12. Room temperature CW X-band EPR spectra of YPO_4:Bi aged for 768 h, YPO_4:Pr aged for 888 h, YPO_4 aged for 432 h and $LaPO_4$ aged for 456 h in Xe excimer discharge lamps, and a control CW X-band EPR spectrum of an empty EPR measurement tube. The simulated EPR spectrum of $LaPO_4$ (red) assumes an S = ½ species interacting with the external magnetic field via an anisotropic g-tensor with components g_x = 2.0057 (0.003), g_y = 2.0160 (0.012) and g_z = 2.0384 (0.034). Values in brackets denote Gaussian distribution widths (strains) accounting for small local variations of the Zeeman interaction. The CW X-band EPR spectra on the right for the aged YPO_4:Bi and YPO_4:Pr samples were collected with a modulation amplitude of 1 G using a power of 0.08 mW at T = 90 K.

As depicted in Fig. 12, aged samples of undoped YPO_4, of YPO_4:Bi and YPO_4:Pr show X-band EPR spectra in the same spectral region as $LaPO_4$. Their EPR line shapes are much more complex than that of aged

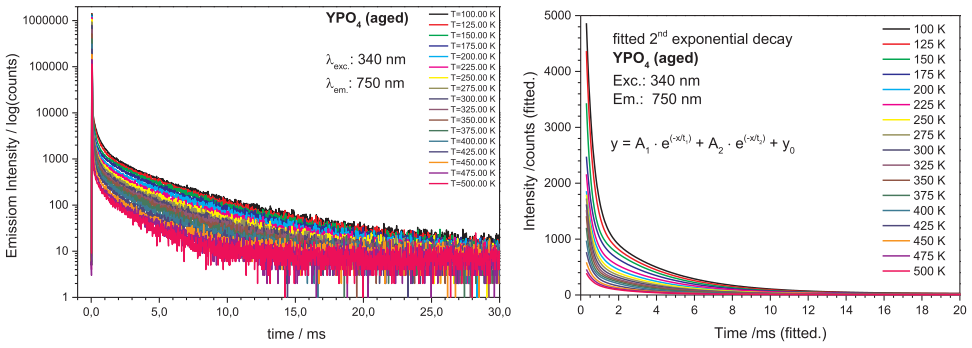

Fig. 11. PL decay temperature map (100 — 500 K) recorded for excimer lamp aged YPO_4 under 340 nm excitation for the 750 nm emission.

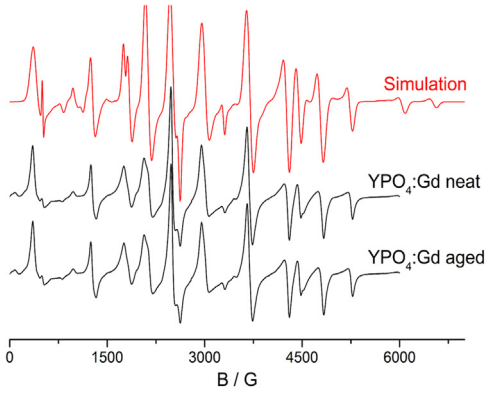

Fig. 13. Room temperature CW X-band EPR spectra: simulated (a) and measured for YPO_4:Gd neat (b) and YPO_4:Gd aged for 2856 h (c) with a modulation amplitude of 5 G using a power of 0.32 mW. For additional details see Supporting Information.

$LaPO_4$. For the Bi- and Pr-doped samples the spectra are virtually identical. To examine whether these spectra arise from a single type of defect or contain multiple components from various species of different chemical nature, we tested for differences in relaxation behaviour by varying the temperature and microwave power of the measurement. Conducting such measurements over the range 90–300 K and 0.08–1.26 mW we found no conclusive evidence for different types of paramagnetic centres, however, this does not disprove the coexistence of different types of defects. Nevertheless the close similarity of the EPR spectra observed for YPO_4:Bi and YPO_4:Pr indicates that the paramagnetic defects formed in these materials are very similar and unrelated to the element that is used as an activator. Furthermore, the spectra closely resemble those obtained on an undoped YPO_4 sample aged under similar conditions. The latter sample also shows some additional features not present in the doped materials revealing different relaxation behaviour. This result points to the presence of some additional defect in the undoped aged YPO_4 host compound that seems to be suppressed in the doped materials. Altogether, our results point to the same aging mechanism involving host structure degradation, in excellent agreement with the conclusion from the absorption and emission spectra discussed above. To clarify the nature of these defects further, complementary low-temperature and pulsed EPR measurements are currently conducted in our laboratory. In the presence of P^{3+}, we would have also expected a P^{4+} signal in the EPR spectrum as a left-over from the conversion of P^{5+} to P^{3+}. Such P^{4+} species were recently observed by Ollier et al. in phosphate glasses as a doublet due to the hyperfine interaction of the unpaired electron with the P-atom in the PO_3^{2-}ion, showing hyperfine splittings between 300 and 1260 G [36]. While our room temperature CW X-band EPR spectra of aged YPO_4:Bi gives no evidence for such a P^{4+} species, a large hyperfine splitting of 500 G can be observed in Fig. 12 for both aged YPO_4 and aged YPO_4:Pr, which could be attributed to such a species.

The spectra of YPO_4:Gd and 2856 h aged YPO_4:Gd are shown in Fig. 13. Gd^{3+} experiences a zero-field splitting due to its group spin $S = 7/2$ and the non-cubic local symmetry in YPO_4:Gd. This interaction is detectable at room temperature and can be measured to probe small changes in the local environment of the activator ion if present. For this purpose CW X-band EPR spectra of the samples YPO_4:Gd and YPO_4:Gd aged were recorded. We find that the activator and its immediate environment are not altered upon aging. The spectra can be simulated with the identical set of parameters, discussed in detail in the Supporting Materials, based on previous single-crystal information [37,38–40]. As the Gd^{3+} signal completely dominates the spectrum defects related to the host signal expected in the 3100–3800 G field range cannot be detected in this case.

4. Conclusions

Microscale powders of YPO_4:Bi, YPO_4:Pr, and YPO_4:Gd are efficient UV emitting materials upon VUV excitation and are thus of interest as radiation conversion screens in Xe excimer discharge lamps. Even though it was assumed that ortho-phosphates are resistant towards the harsh conditions inside a Xe excimer discharge vessel, it turned out that this assumption is not true at all. It turned out that YPO_4 and doped YPO_4 micro-scale phosphor powders degrade just within several hundred hours of Xe excimer lamp operation to such an extent, that commercial use of such UV fluorescent Xe excimer discharge lamps is not in close reach.

The main degradation pathway is a reduction of the reflectance in the UV range accompanied by the formation of a novel luminescent species. Our detailed analysis of degraded materials points to the formation of an s^2-ion type species, which is in line with the type of observed excitation and emission spectra as well as the with analysis of the time dependent behaviour. However, a final proof of our hypothesis requires further spectroscopic investigations, such as temperature dependent EPR spectra and MAS NMR spectra of ^{31}P and ^{89}Y.

Acknowledgement

The authors are grateful to the German Federal Ministry of Education and Research (BMBF) and MB and LF further acknowledge the Foundation of German Economy for generous financial support. Support by FAPESP (CePID project 2013–07793-6) to HE is also acknowledged. Special thanks are due to Prof. Dr. Rainer Pöttgen, WWU Münster for taking some XRD measurements and to the whole Fluoro UV BMBF project team for the fruitful cooperation.

Appendix A. Supplementary material

Supplementary data associated with this article can be found in the online version at http://dx.doi.org/10.1016/j.jlumin.2018.05.056.

References

[1] R.H. Clapp, R.J. Ginther, Ultraviolet phosphors and fluorescent sun tan lamps, J. Opt. Soc. Am. 37 (1947) 355–362.
[2] H.G. Jenkins, A.H. McKeag, P.W. Ranby, Alkaline earth halophosphates and related phosphors, J. Electrochem. Soc. 96 (1949) 1, http://dx.doi.org/10.1149/1.2776766.
[3] M. Koedam, J.J. Opstelten, Measurement and computer-aided optimization of spectral power distributions, Light. Res. Technol. 3 (1971) 205–210, http://dx.doi.org/10.1177/096032717100300303.
[4] J. Verstegen, D. Radielović, L. Vrenken, A new generation of “deluxe” fluorescent lamps, combining an efficacy of 80 lm/W or more with a color rendering index of approximately 85, J. Electrochem. Soc. 121 (1974) 1627–1631, http://dx.doi.org/10.1149/1.2401757.
[5] W. Van Schaik, S.H.M. Poort, J.J.H. Schlotter, E. Dorrestijn, G. Blasse, Influence of Impurities on the Luminescence Quantum Efficiency of the Lamp Phosphor (Ce, Gd, Tb) MgBsO, 0, J. Electrochem. Soc. 141 (1994) 216–222, http://dx.doi.org/10.1149/1.2055087.
[6] B.M.J. Smets, Phosphors based on rare-earths, a new era in fluorescent lighting, Mater. Chem. Phys. 16 (1987) 283–299, http://dx.doi.org/10.1016/0254-0584(87)90103-9.
[7] T. Jüstel, C. Ronda, D. Van der Voort, C.J. Jalink, Low-pressure mercury discharge lamp for tanning, US Patent, US 6,208,069 B1. doi:10.1126/science.Liquids, 2001.
[8] T. Jüstel, C. Ronda, F. Altena, W. Busselt, O. Mastenbroek, H.-.H. Bechtel, Tanning device, US Patent, US 2005/0261751 A1, 2005.
[9] A. Lempicki, A.J. Wojtowicz, E. Berman, Fundamental limits of scintillator performance, Nucl. Inst. Methods Phys. Res. A. 333 (1993) 304–311, http://dx.doi.org/10.1016/0168-9002(93)91170-R.
[10] M. Balcerzyk, Z. Gontarz, M. Moszynski, M. Kapusta, Future hosts for fast and high light output cerium-doped scintillator, J. Lumin. 87– 89 (2000) 963–966, http://dx.doi.org/10.1016/S0022-2313(99)00492-5.
[11] T. Jüstel, H. Nikol, J. Drischerl, D.U. Wiechert, Device for desinfecting water comprising a UV-C Gas Discharge Lamp, US Patent, US 6,398,970 B1.
[12] T. Jüstel, H. Von Busch, G. Heusler, W. Mayr, Device for generating UV radiation, US Patent, US 7,298,077 B2. doi:10.1126/science.Liquids, 2007.
[13] B.T. Jüstel, H. Nikol, Optimization of luminescent materials for plasma display panels, Adv. Mater. 12 (2000) 527–530, http://dx.doi.org/10.1002/(SICI)1521-4095(200004)12:7<527::AID-ADMA527>3.3.CO;2-#.

[14] M. Trevisani, K.V. Ivanovskikh, F. Piccinelli, A. Speghini, M. Bettinelli, Fast UV luminescence of Pr3+- doped calcium lutetium Whitlockite, ECS Trans. (2012) 11–17, http://dx.doi.org/10.1149/1.3697440.
[15] F. Piccinelli, A. Speghini, K. Ivanovskikh, A. Meijerink, C. Ronda, M. Bettinelli, UV and visible luminescence of Pr3+ doped oxides, Mater. Res. Soc. Symp. Proc. 1111 (2009).
[16] R.C. Ropp, Phosphors based on rare earth phosphates fast decay phosphors, J. Electrochem. Soc. 115 (1968) 531, http://dx.doi.org/10.1149/1.2411313.
[17] M. Broxtermann, T. Jüstel, Photochemically induced deposition of protective alumina coatings onto UV emitting phosphors for Xe excimer discharge lamps, Mater. Res. Bull. 80 (2016) 249–255, http://dx.doi.org/10.1016/j.materresbull.2016.04.008.
[18] P. Dorenbos, The Eu3+ charge transfer energy and the relation with the band gap of compounds, J. Lumin. 111 (2005) 89–104, http://dx.doi.org/10.1016/j.jlumin.2004.07.003.
[19] N.R.J. Poolton, A.J.J. Bos, G.O. Jones, P. Dorenbos, Probing electron transfer processes in Y PO 4:Ce, Sm by combined synchrotron–laser excitation spectroscopy, J. Phys. Condens. Matter 22 (2010) 185403, http://dx.doi.org/10.1088/0953-8984/22/18/185403.
[20] P. Dorenbos, 5D level positions of the trivalent lanthanides in inorganic compounds, J. Lumin. 91 (2000) 155–176, http://dx.doi.org/10.1016/S0022-2313(00)00229-5.
[21] R.H.P. Awater, L.C. Niemeijer-Berghuijs, P. Dorenbos, Luminescence and charge carrier trapping in YPO 4:Bi, Opt. Mater. (Amst.). 66 (2017) 351–355, http://dx.doi.org/10.1016/j.optmat.2017.02.032.
[22] A. Lakshmanan, Luminescence and Display Phosphors: Phenomena and Applications, Nova Science Pub Inc., 2007.
[23] R.H.P. Awater, P. Dorenbos, The Bi 3+ 6s and 6p electron binding energies in relation to the chemical environment of inorganic compounds, J. Lumin. 184 (2017) 221–231, http://dx.doi.org/10.1016/j.jlumin.2016.12.021.
[24] G. Blasse, A. Bril, Investigations on Bi 3+ -activated phosphors, J. Chem. Phys. 48 (1968) 217–222, http://dx.doi.org/10.1063/1.1667905.
[25] P. Boutinaud, Revisiting the spectroscopy of the Bi 3+ Ion in oxide compounds, Inorg. Chem. 52 (2013) 6028–6038, http://dx.doi.org/10.1021/ic400382k.
[26] A.M. Srivastava, S.J. Camardello, Concentration dependence of the Bi3+ luminescence in LnPO4 (Ln=Y3+, Lu3+), Opt. Mater. (Amst.) 39 (2015) 130–133, http://dx.doi.org/10.1016/j.optmat.2014.11.011.
[27] L. van Pieterson, M.F. Reid, R.T. Wegh, S. Soverna, A. Meijerink, 4fn > 4fn-15d transitions of the light lanthanides: experiment and theory, Phys. Rev. B. 65 (2002) 45113, http://dx.doi.org/10.1103/PhysRevB.65.045113.
[28] K.-B. Kim, Y.-I. Kim, H.-G. Chun, T.-Y. Cho, J.-S. Jung, J.-G. Kang, Structural and optical properties of BaMgAl 10O17:Eu2+ phosphor, Chem. Mater. 14 (2002) 5045–5052, http://dx.doi.org/10.1021/cm020592f.
[29] M.A. Hughes, Y. Federenko, T.H. Lee, J. Yao, B. Gholipour, R.M. Gwilliam, K.P. Homewood, D.W. Hewak, S.R. Elliott, R.J. Curry, Optical and electronic properties of bismuth-implanted glasses, in: M.J.F. Digonnet, S. Jiang (Eds.): p. 898216. doi:10.1117/12.2036933.
[30] M.L. Passow, M.L. Brake, Production of XeO* in a CW microwave discharge, Plasma Chem. Plasma Process. 9 (1989) 497–511, http://dx.doi.org/10.1007/BF01023916.
[31] A.A. Ionin, L.V. Seleznev, D.V. Sinitsyn, XeO luminescence in a self-sustained slab radio-frequency discharge, Bull. Lebedev Phys. Inst. 35 (2008) 111–112, http://dx.doi.org/10.3103/S1068335608040040.
[32] R.M. Kadam, T.K. Seshagiri, V. Natarajan, S.V. Godbole, Radiation induced defects in BaBPO5:Ce and their role in thermally stimulated luminescence reactions: EPR and TSL investigations, Nucl. Instrum. Methods Phys. Res. Sect. B Beam Interact. Mater. At. 266 (2008) 5137–5143, http://dx.doi.org/10.1016/j.nimb.2008.10.003.
[33] D. Ehrt, P. Ebeling, U. Natura, UV Transmission and radiation-induced defects in phosphate and fluoride–phosphate glasses, J. Non Cryst. Solids 263–264 (2000) 240–250, http://dx.doi.org/10.1016/S0022-3093(99)00681-X.
[34] D.L. Griscom, Electron spin resonance in glasses, J. Non Cryst. Solids 40 (1980) 211–272, http://dx.doi.org/10.1016/0022-3093(80)90105-2.
[35] T.E. Tsai, D.L. Griscom, Experimental evidence for excitonic mechanism of defect generation in high-purity silica, Phys. Rev. Lett. 67 (1991) 2517–2520, http://dx.doi.org/10.1103/PhysRevLett.67.2517.
[36] V. Pukhkaya, F. Trompier, N. Ollier, New insights on P-related paramagnetic point defects in irradiated phosphate glasses: impact of glass network type and irradiation dose, J. Appl. Phys. 116 (2014) 123517, http://dx.doi.org/10.1063/1.4896876.
[37] M. Rappaz, L.A. Boatner, M.M. Abraham, EPR investigations of Gd3+in single crystals and powders of the zircon-structure orthophosphates YPO4, ScPO4, and LuPO4, J. Chem. Phys. 73 (1980) 1095–1103, http://dx.doi.org/10.1063/1.440259.
[38] G. Kuhl, Paramagnetische Resonanz des dreiwertigen Gadoliniums in YPQ, YVQ und YAsO, Z. Phys. 225 (1969) 277–282.
[39] J. Rosenthal, R.F. Rileay, U. Ranon, Electron paramagnetic resonance of Gd3+ in zircon structures. II. YVO4, YPO4, YAsO4, Phys. Rev. 177 (1969) 625–629.
[40] H.G. Kahle, V. Koch, J. Plamper, W. Urban, Zero-field resonance of Gd 3+ in YVO 4 and YPO 4, J. Chem. Phys. 49 (1968) 2702–2703, http://dx.doi.org/10.1063/1.1670473.